Exploring self-writing and photosensitivity in ion-exchanged waveguides

Ami M. Ljungström and Tanya M. Monro

Optoelectronics Research Centre, University of Southampton, Southampton SO17 1BJ, UK

We have demonstrated that self-written channel waveguides can be formed reproducibly in K^+-ion exchanged Nd-doped Bk7 glass by making use of a photosensitive index change of $\sim 6\times10^{-5}$ induced by illumination at 457 nm. The guidance characteristics of these waveguides have been investigated from 457 nm to 1550 nm. Detailed experiments have been carried out exploring the self-writing process, and these are also used to investigate the photosensitivity of the material. We find that an intensity threshold exists below which photosensitivity does not occur. Numerical simulations of both the evolution and guidance properties of the self-written waveguides provide excellent agreement with observations.

OCIS codes: 130.2790, 190.5940, 230.7370, 230.7380.

1. Introduction

Self-written waveguides can evolve if a beam of light is focused onto and allowed to propagate through a photosensitive material.[1–3] A Gaussian beam focused onto a photosensitive sample initially diffracts, and since photosensitive index changes occur

more rapidly where the intensity is high, the material experiences the fastest changes at the input face and along the propagation axis. In many materials light causes the index to increase, which reduces the initial diffraction of the Gaussian writing beam. In the early stages an adiabatic taper forms, and over time a channel waveguide can be induced throughout the sample. These are called *self-written waveguides* (SWWs) as the same light that induces the waveguide is also guided by it.

These waveguides can offer a range of potential advantages over current waveguide fabrication methods such as epitaxial growth, diffusion methods and direct writing.[2] For example, self-writing is a one-step process that requires no translation or chemical processing. In addition, the choice of input beam determines the final waveguide shape. When a Gaussian beam is used, tapers or channels can be self-written, however a more complicated writing beam, for example a multi peaked beam, could ultimately create Y-junctions or couplers.[4] Recent research into self-writing in photopolymers and UV curable resins has shown that Y-junctions can form by using multiple writing beams[5] and also low-loss interconnections between fibers have been self-written.[6,7]

In this paper we explore the self-writing process in planar ion-exchanged silicate glass. Previously self-written channels in planar glass have been created in ion-implanted $Bi_4Ge_3O_{12}$,[8] germanosilicate glass,[1] and As_2S_3 chalcogenide glass.[9,10] In the bulk geometry experiments have been carried out in GLS chalcogenide glass[3] and in Nd-doped Bk7 glass.[11] So far only tapers and channels have been written experimentally in glass, although further progress has been made in photopolymers, largely because photopolymers exhibit reproducible photosensitivity which occurs rapidly (seconds), and large index changes can be obtained (Δn <0.03).[7] This work in poly-

mers demonstrates that self-writing is a powerful technique for creating novel waveguides, and similar improvements in glass would facilitate the development of solid devices with the advantage of ready integration with conventional technologies.

2. Material

In order to be a suitable host for self-writing, a material needs to experience a significant index change in response to light in order to overcome the diffraction of the writing beam and create a waveguide through the glass. In this paper the self-writing process in planar geometry is explored, as this geometry has potential for facile integration with existing planar devices and sources.

We use K^+-ion exchanged Nd-doped Bk7, which has been chosen because Bk7 is a commercially available material with good spatial homogeneity. Also, gratings have been written in planar K^+-ion exchanged silica using 351 nm light to induce index changes of 10^{-5}.[12] Such direct writing processes make use of the absorption of light near the band edge. However, in self-writing, the writing beam must propagate through the whole sample length. Hence light above the band edge can be used to induce a multiphoton absorption process (and thus change the refractive index) without inducing significant loss. However, illumination of K^+-ion exchanged undoped Bk7 at 457 nm or 488 nm using powers below 100 mW did not induce any index changes. We have previously observed that bulk Nd-doped Bk7 glass is both homogeneous and photosensitive, exhibiting a negative index change of 10^{-4} at 488 nm.[11] Therefore we chose to investigate K^+-ion exchanged Nd-doped Bk7 borosilicate glass (1.5-wt% Nd_2O_3), which has previously been used as a host for planar waveguide lasers,[13] and

hence self-writing offers the possibility of integrating passive and active devices.

We observe that this material is photosensitive to both 457 nm or 488 nm light, with the largest effects obtained at 457 nm. It has an initial refractive index of ~1.5 and the ion exchanged planar surface layer has an index difference from the bulk material of 0.0092 and 0.0080 at 1 μm for the TM and TE polarizations respectively.[13] To our knowledge this is the first report of photosensitivity in K^+-ion exchanged Nd-doped Bk7. This material exhibits a high degree of spatial homogeneity, and so we believe that this glass is ideal for exploring self-writing and providing further insights into the photosensitivity mechanisms responsible for the index change.

3. Experiment and experimental results

In these experiments a single mode CW Gaussian output beam at 457 nm from an argon-ion laser is used as the writing beam. The beam is focused to a waist at the polished input face of the 2.5 μm deep ion-exchanged layer. The light initially diffracts through the material, and the beam emerging from the layer is monitored over time. If the refractive index increases due to the illumination, the output beam should narrow and become more intense as the light becomes guided by the waveguide it induces.

As Fig. 1 indicates, the planar ion-exchanged surface layer in this experiment is 2.5 μm deep and here two sample lengths have been used (6.5 and 14 mm). Hence a careful choice of writing beam width is needed: although a more efficient launch into the layer can be obtained using a narrow beam, the layer can not confine such a rapidly diffracting beam well, and also a large index increase is required in order for the self-writing process to overcome the transverse diffraction. Using a circularly

symmetrical beam, a beam with a full width at half maximum (FWHM) of 7 μm is found to offer the best compromise. Note that in the future the use of elliptical writing beams would allow the launch into the layer to be optimized while allowing the transverse width to be specified independently.

Although self-writing using Gaussian writing beams has been conducted in germanosilicate[1] and As_2S_3 chalcogenide[9,10] planar glass, basic self-writing experiments are crucial in any new material to explore the self-writing and photosensitivity processes that occur, and these are presented here for K^+-ion exchanged Nd-doped Bk7.

In Fig. 1 cross sections of the beam emerging from the 6.5 mm long sample are shown during a typical experiment using a 38 mW writing beam. The FWHM of the output beam is observed to narrow over time, here in total by a factor of 7, and becomes more intense by a factor of 2.5. Hence the refractive index must be increasing due to the illumination, which reduces the diffraction of the propagating light that becomes guided through the sample. Note that remarkably good beam quality is obtained, which is a measure of the excellent homogeneity of this glass along the full propagation length. Two different sample lengths, 6.5 and 14 mm, have been used, and unsurprisingly a somewhat higher beam quality is obtained in the shorter sample.

In Fig. 2(a), we can see the change in FWHM at the output face and how it decreases during this exposure. The corresponding increase in peak intensity is shown in Fig. 2(b). Note how the changes slow down at late times in the experiment as the refractive index change saturates and no further changes can be induced. Although the output beam continues to evolve throughout the long exposure time, it is worth noting that the initial change in FWHM is extremely rapid.

The total change in power at the output face is shown in the inset in Fig. 2. In this experiment, a decrease by a factor of 1.4 in power is observed, of which 46% is due to a drop in the power of the writing laser early in the experiment. Comparing the propagation loss through an unexposed region with that in the SWW reveals an equivalent induced loss during the exposure of 1 dB/cm at the writing wavelength (ignoring the change in coupling into the layer due to the induced index change).

During all experiments at 457 nm, a visible red luminescence is generated throughout the sample in positions where the writing beam is intense. The luminescence is found to be dominated by the emission bands around 900, 1060, and 1350 nm characteristic of Nd-doped silica glasses.[14] Since the spatial distribution of the luminescence reflects the intensity distribution of the propagating beam, it could be a useful tool for monitoring the waveguide evolution. In addition it offers useful information about the glass properties, which could be used to explore the photosensitivity of this material.

All the above presented results indicate that this glass is photosensitive at 457 nm and show the key evidence that the index is increasing. We have formed a range of channels within this glass that substantially reduce the diffraction of the propagating beam. Finally, in comparison to previous work,[1] an extremely good beam quality is obtained, which indicates that this glass is well suited for self-writing.

4. Numerical model and simulations

In order to obtain a deeper understanding of the self-writing process, and to predict the effects of different experimental parameters, numerical simulations were conducted. This has previously been done for both planar and bulk geometries.[2,3,11] Here

we define $\Delta n(t, z, x)$ to be the refractive index change in the planar layer due to photosensitivity (see Fig. 1). Note that we assume that the index difference between the layer and the surrounding regions is larger than the index change induced by photosensitivity and thus that Δn is independent of y. Finally, the induced index distribution is taken to initially be uniform throughout the planar layer, i.e. $\Delta n(0, z, x) = 0$.

When the material is illuminated, the locally induced change in refractive index, is described using a phenomenological model for photosensitivity:

$$\frac{\partial \Delta n(t, z, x)}{\partial T} = I^p(t, z, x)\left(1 - \frac{\Delta n(t, z, x)}{\Delta n_s}\right), \tag{1}$$

where the intensity, I, is EE^*, and E is the electric field. A saturation index change, Δn_s, is introduced to limit the change in index that can be induced. This simple phenomenological model has previously shown to agree well with experiments in planar germanosilicate glass.[1] Note that if p=2 a two-photon absorption process occurs within the material. T is a normalized time defined as $T = A_p I_0^p t$, where A_p is a real constant that depends on p, the material properties and the writing wavelength (λ_ω), $I_0 = I(t, 0, x)$, and t is the time in seconds.

In this paper the intensity distribution is taken to be a Gaussian writing beam with a FWHM of $a\sqrt{2\ln 2}$. The paraxial approximation is used to describe light propagation as discussed in Refs 2, 4. As shown in Section 3 the propagation loss increases during the waveguide evolution, and we assume that the loss per unit length is $L_C + L_{PS}$, where L_C is a constant and uniform loss and $L_{PS}(t, z, x) = \gamma k_0 \Delta n(t, z, x)$ is a photosensitivity induced loss, where γ is a constant of proportionality and $k_0 = \frac{2\pi}{\lambda_\omega}$.

This model for the induced loss has previously been shown to agree with experiments in germanosilicate[2] and chalcogenide glass.[3]

The paraxial wave equation and the photosensitivity equation, Eq. (1), along with the writing beam defines the model. In solving these equations, advantage is taken of the difference in time scales between the light propagation (nanoseconds) and the index evolution (minutes), hence the equations can be solved using a split step beam propagation model. When fitting the simulations to experimental data the time in the simulations can be scaled since the normalized time T is used in the model and A_p is unknown. Note that the parameter A_p, and therefore the normalized time, is determined by the details of the material photosensitivity, and hence could be extracted if systematic investigations of a range of experiments were conducted. In most glasses the index change that can be achieved by illumination (typically $10^{-5} - 10^{-2}$) depends critically on the glass composition. Although the change could be measured experimentally we find that self-writing is a powerful tool to extrapolate the magnitude of change of new materials by choosing Δn_s to fit the experiments.

Once the SWWs are formed, the magnitude of the index change can decay slightly over time. In addition, the induced index change is less at longer wavelengths (λ). These effects can be approximated by:

$$\Delta n_{\lambda,t}(\lambda, t, z, x) = D(t)W(\lambda)\Delta n(\lambda_\omega, t_0, z, x), \tag{2}$$

for $t > t_0$ where t_0 is the time when the initial experiment is turned off. $D(t)$ describes the decay in the photosensitive index change, $W(\lambda)$ describes the induced index at

longer wavelengths, and Δn is as defined in Eq. (1). Observe from Eq. (2) that we assume that the index in both cases decreases uniformly throughout the sample.

A. Results and comparison with experiments

In Fig. 2 results from the numerical simulations (grey lines) are shown together with the experiment. Initially any propagation losses were ignored (solid lines) and excellent agreement for the beam width evolution is obtained when the saturation refractive index, Δn_s, is taken to be 5.2×10^{-5} and p=2. However the change in peak intensity shows a significantly larger increase in the simulations than in the experiments.

It has previously been shown[3,4] that loss has a greater influence on the intensity evolution than on the width. By incorporating a photosensitivity induced loss, L_{PS}, in the model, which induces a larger absorption of light at positions where the index has been altered, the right magnitude of intensity change can be induced (dashed lines in Fig. 2). As in Ref. 2, a constant and uniform loss alone does not improve the agreement with experiments significantly. The dashed line corresponds to simulations with Δn_s=5.7×10^{-5} and L_{PS}=90000 $\times\Delta n(z,x)$ dB/cm, i.e. a maximum loss of 5.13 dB/cm is present at positions where Δn_s is reached. However, in reality a constant and uniform propagation loss, L_C, is also present in the material and by including both type of losses the agreement could be improved even further for the evolution in both FWHM and peak intensity, as shown by the dotted lines in Fig 2. Here the (fitted) material parameters are Δn_s=5.7×10^{-5}, L_C=2 dB/cm and L_{PS}=85000 $\times\Delta n(z,x)$ dB/cm, hence a maximum L_{PS} of 4.85 dB/cm occurs at localized positions where Δn_s has been reached. Although these losses appear to be high,

the regions of high loss are localized and our experiments indicate that the total loss induced at the writing wavelength is 1 dB/cm.

In Fig 3(a) the beam emerging from the shorter sample at the end of the experiment (solid line) is reproduced from Fig. 1 along with the corresponding simulation using the fitted material parameters, dotted line. The originally Gaussian distribution grows a pedestal in both experiment and simulation during the evolution.

Good agreement is also obtained for experiments carried out in the longer sample using the same parameters as above, see Fig. 4 for the first 175 hours exposure using a power of 20 mW. The fact that our model also agrees with experiments in this longer sample confirms that this is an excellent model for self-writing and that these material parameters describe the photosensitivity of K^+-ion exchanged Nd-doped Bk7 well.

In the experiments the evolution of the refractive index is determined indirectly by monitoring the propagating writing beam at the output face. However, since Fig. 2-4 show good agreement between experiments and simulations, the numerical simulations can be used as a tool for extracting information about the evolution of the refractive index distribution within the material. In Fig. 3(b) and (c) the index distributions from the simulation are shown for two different times during the evolution, equivalent to 140 and 420 hours in the experiment in the shorter (6.5 mm long) sample shown in Fig. 2. The cross sections along the propagation axis show that the index initially grows more quickly near the input face where the light intensity is highest and how it over time penetrates further along the propagation axis into the material.

The above results prove K^+-ion exchanged Nd-doped Bk7 to be photosensitive to light at 457 nm and that waveguides can be self-written in this glass. The sample is

found to be homogeneous throughout the whole layer, which makes it straightforward to locate the channel after the exposure, and also to reproduce the experiments. In addition, since different samples have been used it has proven to be a reliable and consistent material. Consequently it promises to be an excellent host for self-writing, offering the possibility of extending and developing the self-writing process further. The fact that the numerical simulations describe the different experiments extremely well using physically reasonable values for the material parameters, validates the simple phenomenological model used. Finally, these results provide useful information about the photosensitivity mechanisms occurring during the self-writing process.

5. Investigation of photosensitivity

A. Decay of index change

To investigate whether the induced photosensitive index changes are permanent a beam was sent through the waveguide after the initial exposure. Any decay in index can be observed by monitoring the increase in the FWHM over time. Fig. 5(a) shows that a small decay in index is present over a time scale of several weeks. Note that the sample was not annealed, a technique that is often used to fix the index change.

This technique monitors the change in index *indirectly*. In order to extract the magnitude of this decay the simulations can be used to determine the relationship between index change and output beam width. This is done by applying a spatially uniform decay of a factor of $D(t)$ as in Eq. (2) to the index distribution created in our simulations. By propagating light through this modified index distribution, we can link the index decay to the FWHM of the output beam, as shown by the inset in

Fig. 5(a), where $\Delta n_{\lambda,t}(\lambda, t, 0, 0)$ is the largest index change present in the structure (which is in general Δn_s). Even when the index change has decayed to half its original value, here 2.85×10^{-5}, the beam width has only increased by 15%.

In Fig. 5(b) the widths from the re-exposures shown in (a) have been converted into index change using the above mapping, which shows that on a time scale of months an index change of 4.25×10^{-5}, i.e. 75%, is still present. Note that the time in this graph is measured from the point where the initial experiment was turned off. The decay in refractive index can be described using a model previously applied to investigate the relaxation of photosensitive index changes in UV induced fiber Bragg gratings:[15] $\Delta n_{\lambda,t}(\lambda, t, 0, 0) = 1 - at^b + c$, where a, b and c are constants chosen to fit the experimental data. This numerical fit is shown as the solid line in Fig. 5(b), where a=1.04×10^{-6}, b=0.24 and c=-0.999942. In order to predict the long term aging effects, this model was used to extrapolate the decay in the induced refractive index (see inset in Fig. 5(b)). Even after a decade nearly half of the index change still remains, which shows that the waveguide would still reduce the diffraction of a propagating beam by a factor of nearly 3.5 relative to free diffraction.

B. Dependence on writing power

As mentioned earlier we find K^+-ion exchanged Nd-doped Bk7 to be very homogeneous, and therefore the photosensitivity in this material can be investigated in more detail. Photosensitive index changes are known to occur more rapidly as the power increases although it is difficult to monitor the change directly. Self-writing can be used as a tool to investigate the relationship between power and speed of index change

and here the early stages of waveguide evolution are studied, where the index change has not yet saturated. In addition, in these early times the greatest increase in index is induced at the input face, which acts as a focusing lens, and the reduced diffraction of the propagating writing beam reflects the strength of this lens.

Here the initial change in FWHM at the output face of the sample is monitored during a 1 hour experiment using different writing powers (for a fixed writing beam width). Results for a 7 μm beam in a 14 mm long sample are shown by the stars in Fig. 6(a). Note that the change in width reflects the magnitude of induced refractive index increase. It is evident that the process proceeds faster at higher powers. This is consistent with the numerical model for the photosensitivity described by Eq. (1), where the index change depends on the intensity squared for this 2-photon absorption process, and corresponding numerical simulations, dotted line, verify this. In addition the experimental results reveal a threshold in writing power at approximately 5 mW: no index changes are induced at lower powers. The smoothness of this experimentally obtained curve reflects the excellent homogeneity of our sample (since each data point corresponds to a different part of the sample).

To gain a fuller understanding of these results, the same experiments were also performed for a wider beam with a FWHM of 12.5 μm. This is shown by the dots in Fig. 6(a), and corresponding simulation results are shown by the the dotted line. A threshold in power is again observed, this time at a higher power of 7 mW. When comparing the two sets of experiments, a steeper curve (and therefore faster process) is evident for the narrower beam. This is not surprising because the narrower beam has a higher peak intensity at the same writing power. Note that the peak intensities

corresponding to the power threshold differ for the two beam sizes.

As described above, good agreements between experiments and simulations were obtained for both beam sizes when using higher powers, however this numerical model for the index change can not reproduce the observed threshold behavior. Indeed, the simple model in Section 4 always induces the same final index distribution regardless of the peak intensity (although longer times are needed for lower intensities), and so a new model is required to describe the threshold. This new model must significantly modify the index change near the threshold so as to enhance the change just above the threshold and reduce it sharply below. It must also exhibit the same behavior at high intensities as the simple model. This can be achieved by modifying Eq. (1) in the following manner:

$$\frac{\partial \Delta n}{\partial T} = \left| I^2 + \alpha I \tanh\left(\frac{\beta}{I - I_{thres}}\right) \right| \left(1 - \frac{\Delta n}{\Delta n_s}\right), \tag{3}$$

where α and β are chosen to fit the experimental data. I_{thres} is an intensity threshold derived from the measured power threshold. When comparing the results using this model with the experiments an excellent agreement for the speed of the process is obtained for both widths, solid lines in Fig. 6, where α=600 and β=0.002.

Although it is likely that a similar threshold behavior could be induced using other models, we found this to be the simplest model resulting in a good agreement with experiments. In addition this modified model gives similarly good agreement as the original model for the total waveguide evolution (not shown here for brevity). Note that when operating close to the material threshold, separate simulations will

be needed for different writing powers. However, at high powers the simpler original model gives good results, hence the threshold can be ignored. The accurate prediction of the observations for all the data suggests that the model describes the material well and is likely to be a useful tool for investigating photosensitivity not only for the development of SWWs, but also for writing gratings or other photolithography applications such as direct writing techniques.

6. Guiding light in the self-written waveguide

A. Experimental observations

In order to investigate the guidance properties of the waveguides self-written in our experiments, Gaussian beams of different sizes and light at longer wavelengths were launched into the structure. During the initial experiment a writing beam with a FWHM of 7 μm at 457 nm was used, and the resulting SWW reduced the diffraction of light by a factor of 7. Here beams with FWHM ranging between 2.5-7 μm are launched into the waveguide. The effect of the SWW on the launched beams is quantified by measuring the *reduced diffraction*, which is defined to be the ratio between the width of a beam emerging from an unexposed region to that emerging from the waveguide. In Fig. 7(a) the dots show the result of this investigation at 457 nm. This reveals a more dramatic light confinement for narrower beams, which is due to the fact that narrow beams exhibit a larger free diffraction than that of wider beams, hence a greater reduction in diffraction is possible. However, for the narrowest beams, the waveguide is not strong enough to entirely confine this rapidly diffracting beam. A good example of a narrow but still well confined beam is obtained using a 3 μm beam,

see graph (a) in Fig. 8 where a cross section of the beam emerging from the waveguide is shown, dashed line. It is clear that the light is well confined in the channel when this data is compared with the equivalent beam diffracting in a uniform material (solid line). Note that these experiments were carried out at powers well below the threshold, hence no further index changes were induced during characterization.

These SWWs will ultimately be most useful at longer wavelengths where the index change will be somewhat lower than at the writing wavelength (457 nm). Here light at longer wavelengths are launched into the SWW in order to determine the guidance properties, and also extract the index change at these wavelengths. In Fig. 8, graph (b), we can see that good confinement of light is also obtained at 633 nm, here for a beam with a FWHM of 3.6 μm. The summary in Fig. 7(a) shows that very similar guidance is obtained at 457 and 633 nm. At 1047 nm and 1550 nm a somewhat weaker guidance is found, although a significant reduction by a factor of 3 is still present at 1047 nm, which shows that these waveguides guide light over a broad wavelength band. In addition, the photo-induced loss through the channel is significantly smaller at the longer wavelengths; at 633 nm the induced loss is 0.5 dB/cm and at 1047 nm it is 0.25 dB/cm, in comparison to 1 dB/cm at the writing wavelength (the difference in coupling to the waveguide at different wavelengths has been ignored).

Finally the sample was turned around and light launched in from the back of the SWW. This results in a strong confinement of the central part of the beam, see (c) and (d) in Fig. 8 for 457 and 633 nm. Observe that some of the light remains in a low level pedestal. The reason why not all the light gets trapped is due to the fact that the SWW is not uniform, i.e. the index difference at the end is not as large as at the

beginning, recall Fig. 3(b) where the index distribution is shown. Hence, since the propagating light diffracts rapidly close to the input face, where the index difference now is relatively small, less light is confined to the waveguide. However, still 25% of the power at the output face is trapped in the center peak and at both 457 and 633 nm, using an input beam width of 4 μm and 3.6 μm respectively, an enormous reduced diffraction by a factor of 40 is obtained, largely due to the high index change near the original input face which acts as a lens. This result in a more uniform waveguide for the light that does get trapped: the propagating light is observed only to grow in width by a factor of 1.2 from input to output at 457 nm and by a factor of 2 at 633 nm, compared with 5 and 7 when front launching.

B. Comparison with numerical simulations

In order to compare the results in the previous section with simulations, light is allowed to propagate through the index distribution calculated from the full simulations presented in Section 4. In Fig. 7(b) the numerical results corresponding to the experiments (presented to the left) are shown. At 457 nm, dots, and at 633 nm, stars, an excellent agreement between experiment and simulations is obtained, which shows that no degradation of the index change is present at 633 nm. In addition this is a powerful test of the numerical model used, which confirms that the simulations do indeed create a refractive index distribution similar to that formed in the experiment, and that the numerically induced spatial distribution in the index change is accurate, since differently sized beams propagate in the same way as observed experimentally. Note also that no free parameters exist in these simulations. In addition this shows

that the model describing the time evolution in this cumulative process is valid.

As already mentioned, at longer wavelengths the effective index change is typically smaller than at the writing wavelength and this can also be quantified using the numerical simulations. At 1047 and 1550 nm the magnitude of index change is decreased according to Eq. (2) in Section 4. If it is reduced to 45% of its original value, i.e. $W(\lambda)$=0.45 hence Δn_s=2.6×10^{-5}, good agreement with experiments at 1047 nm can be obtained, see triangles in Fig. 7. The equivalent result for light at 1550 nm is shown by the circles and here the index needs to be reduced to 40% of the original change, i.e. Δn_s=2.3×10^{-5}, to fit the experiments. The good agreement with experiments indicates that the guidance at all wavelengths within the SWW can be described by making this straightforward modification to the numerical model.

Numerical simulations have also been carried out corresponding to the experiments when launching light in from the back of the sample. Here a qualitative agreement is obtained. We believe that possible differences in the induced index distributions formed in the simulations, to that in the experiment, accumulate further into the material and the largest discrepancies will be found at the output face. Also small imperfections in the glass are more noticeable where the index change is smaller, i.e. close to the output face. Hence although when sending light in from the front these errors are negligible, they will have a larger effect when launching light in from behind.

7. Optimizing the self-writing process

For a given beam, the structure that evolves is determined by the achievable index change in the material: using a Gaussian beam, channels form if the material exhibits

a large enough increase to totally overcome the diffraction, otherwise the evolution stops earlier and a taper forms. Here we use our experimentally validated simulations to predict whether tapers or channels form for a range of experimental conditions. This is done for a 1 cm long sample, and losses in the material are ignored for simplicity.

The structure that results using our experimental parameters (FWHM 7 μm, writing wavelength 457 nm) can be seen in (a) in Fig. 9(left). This structure tapers in width by a factor of 1.7 in the 1 cm long sample. To investigate ways of making more uniform channels, we perform simulations to explore the SWWs that form for a range of different values of the writing FWHM and saturation index change. Using these simulations, we identify the conditions under which a relatively uniform channel waveguide forms, where a channel is here defined as a refractive index distribution that tapers in width by less than a factor of 1.2 from input to output. Using this definition, experiments located above the curve in Fig. 9(right) result in channels, whereas below the curve tapers are formed. Note that the relationship between the writing FWHM and the width of the resulting channel is nearly linear, see inset.

See from Fig. 9(right) that although our experiment (a) produced a tapered waveguide, a channel can form in this material using a wider beam, for example 9 μm, as in (b). Using a material with a slightly larger index change of 9×10^{-5}, narrower channels can be created as shown by (c). From this it is evident that to form narrow channels, a material with a large index change is required. This is due to the fact that narrow beams diffract more rapidly than wider beams and hence a larger change is needed in order to counteract this diffraction. We can see in the graph that the possible self-written channel widths are in the range suitable for integration

with fibers and other devices and that relatively small index changes are needed in order to write these waveguides. Note also that the photosensitivity of the material used here has not been optimized and we believe that by exploring the Nd-dopant concentration and the potassium concentration the index change could be increased.

8. Discussion and Conclusion

In this paper the photosensitivity process in K^+-ion exchanged Nd-doped Bk7 is investigated. This material exhibits a refractive index increase of 5.7×10^{-5} under illumination at 457 nm using powers up to 40 mW. In comparison to most previous self-writing experiments reported in glass, our material is found to exhibit the excellent homogeneity required to successfully reproduce the experiments and compare results using different experimental parameters. This has allowed information about the photosensitivity process occurring within the material to be extracted. This material exhibits a power threshold in photosensitivity that depends on the beam size; using a writing beam of 7 μm no index changes are induced below 5 mW and for a wider beam of 12.5 μm the threshold is 7 mW. The physical mechanism that causes this threshold is at present unclear. Investigations of the sample input face using a microscope reveal that no obvious physical damage occurs during the exposure. It is possible that the threshold could exist because a finite energy is required to cause structural rearrangements, and thus change the refractive index. In practice, this threshold is useful when characterizing the waveguide after the exposure, since low power illumination does not induce additional changes. This is particularly important in a material like the one used here where the early index changes occur rapidly.

The self-writing process proceeds faster at higher peak intensities, hence using a higher writing power increases the writing speed, although of course increasing it dramatically will ultimately damage the sample. Another way of increasing the peak intensity is by using a narrower writing beam and as long as a sufficient index change is possible in the sample, narrower waveguides could be written at higher speeds.

Investigations of the aging of the induced index changes have been carried out. This revealed that the index changes are long lasting and that half of the change will remain for at least a decade. In addition the waveguides can be used to guide light at longer wavelengths: they guide well at 633 nm, although the guidance at 1047 and 1550 nm is somewhat weaker. The guidance at these longer wavelengths could be improved if slightly larger index changes were induced, which would be possible by optimizing the photosensitivity within the material.

We have also shown that numerical simulations of the process describe the experiments well. When modeling experiments that are carried out close to the power threshold a modification to the model that incorporates this property is needed. Here a suitable model has been developed which provides good agreement with experiments.

Note that in all simulations carried out the index changes are assumed only to affect the beam in the transverse direction. Although the excellent agreements with experiments show that this assumption is reasonable, it could be possible in the future to carry out bulk simulations taking into account the alterations in launch conditions into the layer. In addition, we have previously found that bulk Nd-doped Bk7, used as host to the planar ion-exchanged layer, exhibits a decrease in index when exposed to blue light.[3] Since some of the propagating light will illuminate the bulk of the material

during the self-writing process this will also affect the launch conditions as the index difference between layer and bulk therefore increases during the illumination.

Due to the excellent agreement between experiment and simulations throughout this paper the numerical simulations have been used to investigate how the choice of different experimental parameters influences the final waveguide structure. This shows that when a Gaussian writing beam is used in a material with a certain possible index change, the resulting structure depends critically on the writing beam size, which determines whether a channel or taper will form in response to the illumination.

Our observations indicate that K^+-ion exchanged Nd-doped Bk7 is an ideal host for self-writing experiments. Here we have developed a reliable numerical model that describes self-writing in this material well, and, when used in conjunction with experiments, can be used to characterize the photosensitivity of the material. Hence we anticipate that this material should provide a platform for developing the self-writing process further in glass. Since the photosensitivity of this material has not been optimized it is likely that larger index changes should be possible. Ultimately, self-writing should allow the formation of waveguide structures that can be directly integrated with existing devices. In addition, it offers the prospect of forming complex, low-loss, waveguide structures without translating either the sample or the writing beam.

Acknowledgements

We thank Dave Shepherd and Simon Hettrick, Optoelectronics Research Centre, University of Southampton, for their help in fabricating the glass samples and also for helpful discussions. Tanya Monro acknowledges the support of a Royal Society URF.

References

1. T. M. Monro, D. Moss, M. Bazylenko, C. M. de Sterke, and L. Poladian, "Observation of self-trapping of light in a self-written channel in photosensitive glass," Phys. Rev. Lett. **80**, 4072-4075 (1999).
2. T. M. Monro, C. M. de Sterke, and L. Poladian, "Investigation of waveguide growth in photosensitive germanosilicate glass," J. Opt. Soc. Am. B **13**, 2824-2832 (1996).
3. A. M. Ljungström, and T. M. Monro, "Light-induced self-writing effects in bulk chalcogenide glass," J. Lightw. Tech. **20**, 78-85 (2001).
4. T. M. Monro, C. M. de Sterke, and L. Poladian, "Analysis of self-written waveguide experiments," J. Opt. Soc. Am. B **16**, 1680-1685 (1999).
5. S. Shoji, S. Kawata, A. A. Sukhorukov, and Y. S. Kivshar, "Self-written waveguides in photopolymerizable resins," Opt. Lett. **27**, 185-187 (2002).
6. S. S. Sarkisov, V. Grimalsky, M. J. Curley, G. Adamovsky, and C. Martin, "Connection of two-dimensional optic fibre arrays using optical beam self-trapping in photocurable media," Proc. SPIE **4455**, 107-118 (2001).
7. N. Hirose, and O. Ibaragi, "Optical solder effect in self-written waveguides in optical circuit devices coupling," Elec. Comp. Tech. Conference (2002).
8. W. S. Brocklesby, S. J. Field, D. C. Hanna, A. C. Large, J.R. Lincoln, D. P. Shepherd, and A. C. Tropper, "Optically written waveguides in ion implanted $Bi_4Ge_3O_{12}$," Opt. Mat. **1**, 177-184 (1992).
9. C. Meneghini, and A. Villeneuve, "As_2S_3 photosensitivity by two-photon absorp-

tion: holographic gratings and self-written channel waveguides," J. Opt. Soc. Am. B **15**, 2946-2950 (1998).

10. N. Hô, J. M. Laniel, R. Vallée, and A. Villeneuve, "Creation of microchannels in a photosensitive As_2S_3 slab waveguide," J. Opt. Soc. Am. B **19**, 875-880 (2002).
11. A. M. Ljungström, and T. M. Monro, "Observation of light-induced refractive index reduction in bulk glass and application to the formation of complex waveguides," Opt. Express **10**, 230-235 (2002).
12. J. E. Roman, and K. A. Winick, "Photowritten gratings in ion-exchanged glass waveguides," Opt. Lett. **18**, 808-810 (1993).
13. S. J. Hettrick, J. I. Mackenzie, R. D. Harris, J. S. Wilkinson, D. P. Shepherd, and A. C. Tropper, "Ion-exchanged tapered-waveguide laser in neodymium-doped BK7 glass," Opt. Lett. **25**, 1433-1435 (2000).
14. S. B. Poole, D. N. Payne, R. J. Mears, M. E. Fermann, and R. I. Laming, "Fabrication and characterization of low-loss optical fibers containing rare-earth ions," J. Lightwave Technol. **LT-4**, 870-875 (1986).
15. T. Erdogan, V Mizrahi, P. J. Lemaire, and D Monroe, "Decay of ultraviolet-induced fiber Bragg gratings," J. Appl. Phys. **76**, 73-80 (1994).

List of Figure Captions

Fig. 1. Left: Light propagates in the 2.5 μm deep ion-exchanged layer. Right: Output beam profiles during waveguide evolution (writing wavelength: 457 nm, power: 38 mW, FWHM: 7 μm, sample length: 6.5 mm).

Fig. 2. Change in FWHM and peak intensity at the output face for the experiment shown in Fig. 1 (black) and corresponding simulations (grey). Solid lines ignore loss, dashed lines include L_{PS} and dotted lines include both L_{PS} and L_C (see text). The inset shows the change in power during the experiment.

Fig. 3. (a) Final output beam shapes in the 6.5 mm sample, solid line experiment and dotted line simulation using fitted material parameters. (b) and (c) simulated index distribution during evolution (the contour levels are separated by 2 dB and the transverse distance has been scaled; only the central 0.3 mm region is shown) and cross sections of the index along the propagation axis.

Fig. 4. Experimental and numerical results (using fitted material parameters) from the longer (14 mm) sample during the first 175 hours, here power=20 mW.

Fig. 5. (a) Initial experiment together with re-exposures. The inset shows the relationship between output FWHM and Δn. (b) Corresponding decay in index after the initial exposure, and a numerical fit. The inset shows the index decay prediction over a time scale of years.

Fig. 6. Speed of process at different input powers during the first hour of exposure. Stars: experiment using a 7 μm beam and dots: 12.5 μm beam. Dotted lines show corresponding simulation using the original numerical model and solid lines the

model including an intensity threshold. Note that all simulations assume p=2 and Δn_s=5.2×10^{-5}, and no loss.

Fig. 7. Reduced diffraction in the self-written waveguide in comparison to a uniform material for a range of beam sizes.

Fig. 8. Beams emerging from the waveguide, dashed lines, and propagating in a uniform material, solid lines. (a) Front launch at 457 nm using an input FWHM of 3 μm. (b) Front launch at 633 nm using a FWHM of 3.6 μm. (c) Back launch into the waveguide at 457 nm and (d) back launch at 633 nm.

Fig. 9. Left: Index distribution for (a) FWHM=7 μm, Δn_s=5.2×10^{-5} as in our experiment, (b) FWHM=9 μm, Δn_s=5.2×10^{-5} and (c) FWHM=7 μm, Δn_s=9×10^{-5}. Right: Waveguide shape as a function of FWHM and Δn_s: above the curve, channels are formed and below tapers are obtained. The inset shows the relationship between FWHM and resulting channel width.

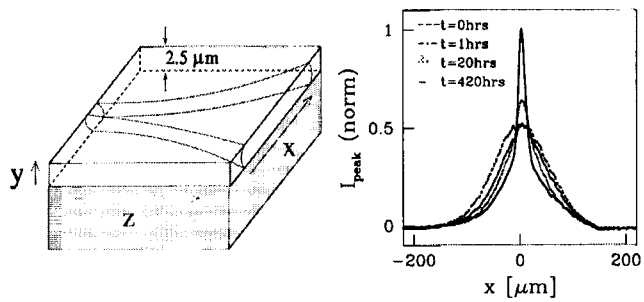

Fig. 1. Left: Light propagates in the 2.5 μm deep ion-exchanged layer. Right: Output beam profiles during waveguide evolution (writing wavelength: 457 nm, power: 38 mW, FWHM: 7 μm, sample length: 6.5 mm). ljungstrom1.eps.

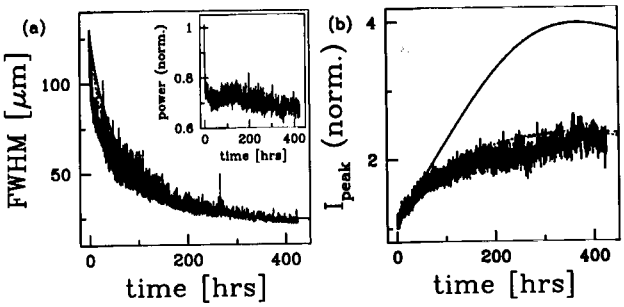

Fig. 2. Change in FWHM and peak intensity at the output face for the experiment shown in Fig. 1 (black) and corresponding simulations (grey). Solid lines ignore loss, dashed lines include L_{PS} and dotted lines include both L_{PS} and L_C (see text). The inset shows the change in power during the experiment. ljungstrom2.eps.

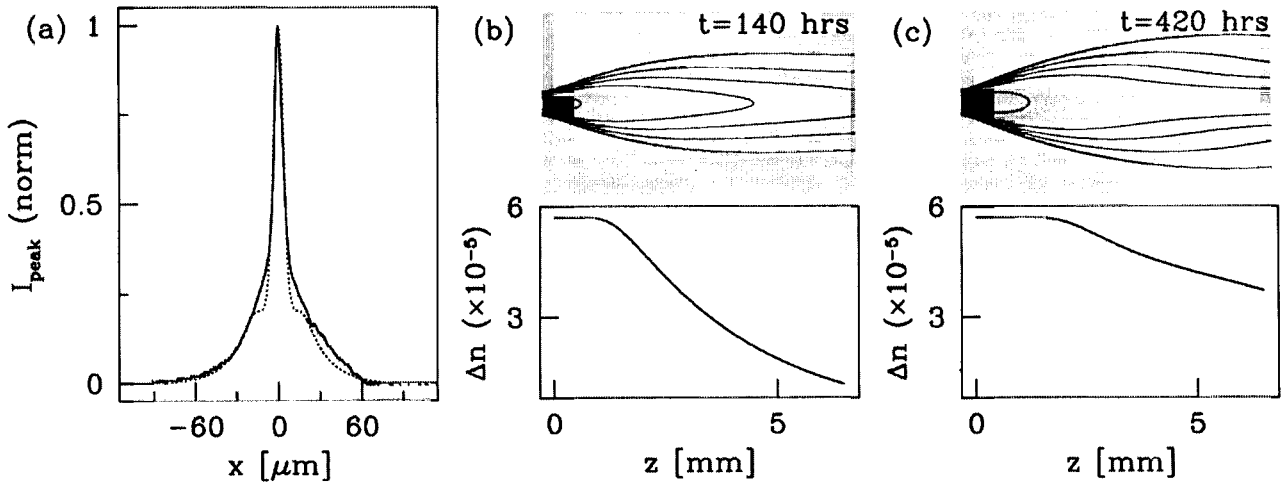

Fig. 3. (a) Final output beam shapes in the 6.5 mm sample, solid line experiment and dotted line simulation using fitted material parameters. (b) and (c) simulated index distribution during evolution (the contour levels are separated by 2 dB and the transverse distance has been scaled; only the central 0.3 mm region is shown) and cross sections of the index along the propagation axis. ljungstrom4.eps.

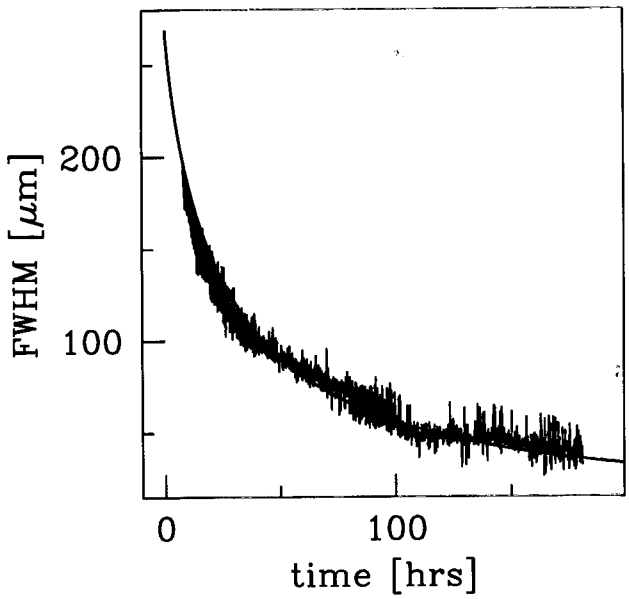

Fig. 4. Experimental and numerical results (using fitted material parameters) from the longer (14 mm) sample during the first 175 hours, here power=20 mW. ljungstrom3.eps.

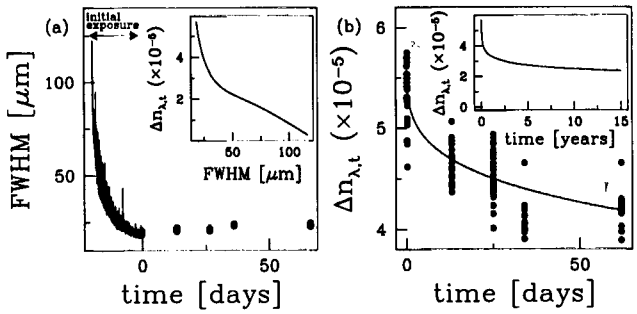

Fig. 5. (a) Initial experiment together with re-exposures. The inset shows the relationship between output FWHM and Δn. (b) Corresponding decay in index after the initial exposure, and a numerical fit. The inset shows the index decay prediction over a time scale of years. ljungstrom5.eps.

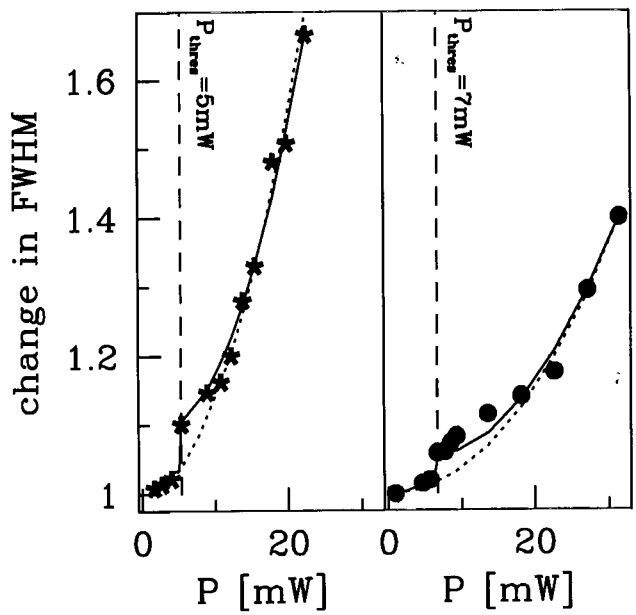

Fig. 6. Speed of process at different input powers during the first hour of exposure. Stars: experiment using a 7 μm beam and dots: 12.5 μm beam. Dotted lines show corresponding simulation using the original numerical model and solid lines the model including an intensity threshold. Note that all simulations assume p=2 and Δn_s=5.2×10^{-5}, and no loss. ljungstrom6.eps.

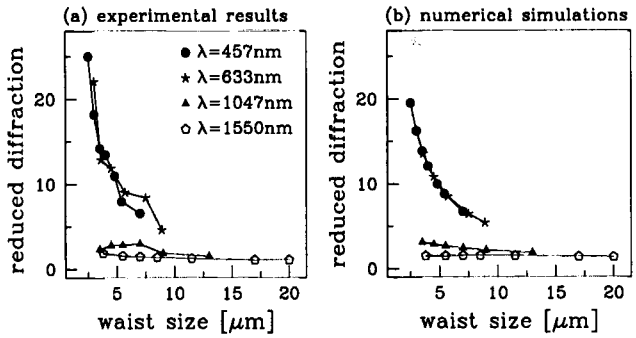

Fig. 7. Reduced diffraction in the self-written waveguide in comparison to a uniform material for a range of beam sizes. ljungstrom7.eps.

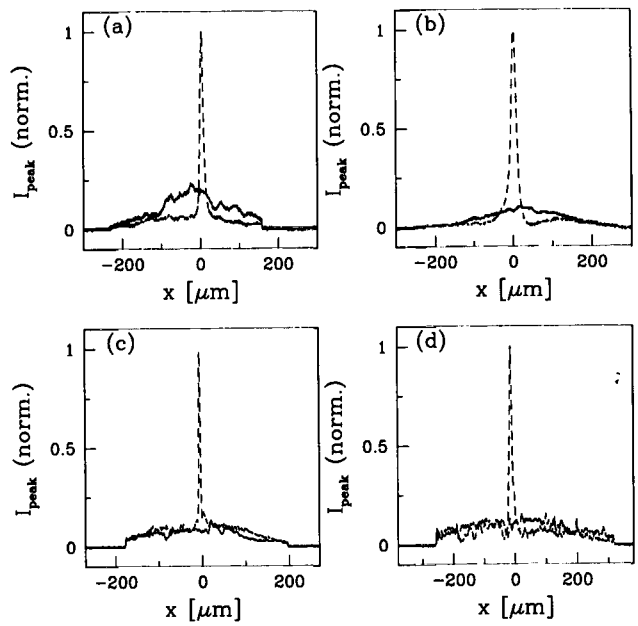

Fig. 8. Beams emerging from the waveguide, dashed lines, and propagating in a uniform material, solid lines. (a) Front launch at 457 nm using an input FWHM of 3 μm. (b) Front launch at 633 nm using a FWHM of 3.6 μm. (c) Back launch into the waveguide at 457 nm and (d) back launch at 633 nm. ljungstrom8.eps.

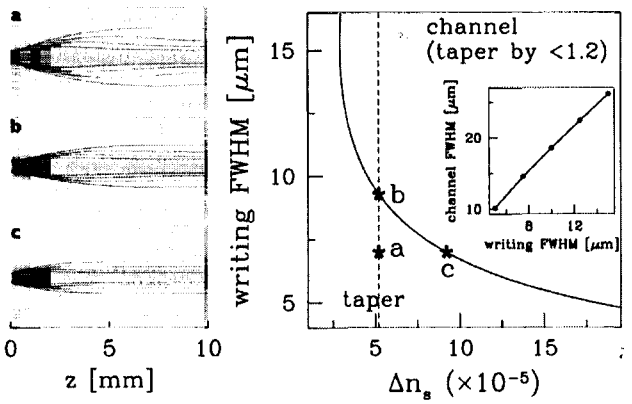

Fig. 9. Left: Index distribution for (a) FWHM=7 μm, Δn_s=5.2×10^{-5} as in our experiment, (b) FWHM=9 μm, Δn_s=5.2×10^{-5} and (c) FWHM=7 μm, Δn_s=9×10^{-5}. Right: Waveguide shape as a function of FWHM and Δn_s: above the curve, channels are formed and below tapers are obtained. The inset shows the relationship between FWHM and resulting channel width. ljungstrom9.eps.